UNIVERSIDADE ESTADUAL DE CAMPINAS
SISTEMA DE BIBLIOTECAS DA UNICAMP
REPOSITÓRIO DA PRODUÇÃO CIENTIFICA E INTELECTUAL DA UNICAMP

Versão do arquivo anexado / Version of attached file:

Versão do Editor / Published Version

Mais informações no site da editora / Further information on publisher's website:

https://www.osapublishing.org/boe/abstract.cfm?uri=boe-8-3-1575

DOI: 10.1364/BOE.8.001575

Direitos autorais / Publisher's copyright statement:

Multimodal evaluation of ultra-short laser pulses treatment for skin burn injuries

Moises Oliveira dos Santos,[1,2] Anne Latrive,[2] Pedro Arthur Augusto de Castro,[2] Wagner de Rossi,[2] Telma Maria Tenorio Zorn,[3] Ricardo Elgul Samad,[2] Anderson Zanardi Freitas,[2] Carlos Lenz Cesar,[4,5] Nilson Dias Vieira Junior,[2] and Denise Maria Zezell[2,*]

[1]*Universidade do Estado do Amazonas, Escola Superior de Tecnologia, Manaus, AM, Brazil*
[2]*Instituto de Pesquisas Energeticas e Nucleares, Centro de Lasers e Aplicacoes, Sao Paulo, SP, Brazil*
[3]*Universidade de Sao Paulo, Instituto de Ciencias Biomedicas, Sao Paulo, SP, Brazil*
[4]*Universidade Estadual de Campinas, Instituto de Fisica Gleb Wataghin, Campinas, SP, Brazil*
[5]*Universidade Federal do Ceara, Departamento de Fisica, Fortaleza, CE, Brazil*
[*]*zezell@usp.br*

Abstract: Thousands of people die every year from burn injuries. The aim of this study is to evaluate the feasibility of high intensity femtosecond lasers as an auxiliary treatment of skin burns. We used an *in vivo* animal model and monitored the healing process using 4 different imaging modalities: histology, Optical Coherence Tomography (OCT), Second Harmonic Generation (SHG), and Fourier Transform Infrared (FTIR) spectroscopy. 3 dorsal areas of 20 anesthetized Wistar rats were burned by water vapor exposure and subsequently treated either by classical surgical debridement, by laser ablation, or left without treatment. Skin burn tissues were non-invasively characterized by OCT images and biopsied for further histopathology analysis, SHG imaging and FTIR spectroscopy at 3, 5, 7 and 14 days after burn. The laser protocol was found as efficient as the classical treatment for promoting the healing process. The study concludes to the validation of femtosecond ultra-short pulses laser treatment for skinburns, with the advantage of minimizing operatory trauma.

References and links

1. American Burn Association, "Burn incidence and treatment in the United States: 2016 fact sheet. 2016," http://www.ameriburn.org/resources_factsheet.php (2016).
2. K. E.Kadler, D. F.Holmes, J. A.Trotter, and J. A.Chapman, "Collagen fibril formation." Biochem. J. **316**, 1–11 (1996).
3. A. L. Kierszenbaum, *Histology and cell biology: an introduction to pathology*, 2nd ed (Mosby Elsevier, 2007).
4. B. S. Atiyeh, S. W. Gunn, and S. N. Hayek, "State of the art in burn treatment," Phys. Med. Biol **29**, 131–148 (2005).
5. A. Vogel and V. Venugopalan, "Mechanisms of pulsed laser ablation of biological tissues," Chem. Rev. **103**, 577–644 (2003).
6. W.Drexler and J. G. Fujimoto, *Optical Coherence Tomography: Technology and Applications*, 2nd ed. (Springer, 2015).
7. W. Drexler, M. Liu, A. Kumar, T. Kamali, A. Unterhuber, and R. A. Leitgeb, "Optical coherence tomography today: Speed, contrast, and multimodality," J. Biomed. Opt. **19**, 71412 (2014).
8. A. I. Kholodnykh, I. Y. Petrova, S. Member, M. Motamedi, and R. O. Esenaliev, "Accurate measurement of total attenuation coefficient of thin tissue with optical coherence tomography," IEEE J. Sel. Top. Quantum Elec. **9**, 210–221 (2003).
9. D. J. Faber, F. J. van der Meer, M. C. G. Aalders, and T. G.van Leeuwen, "Quantitative measurement of attenuation coefficients of weakly scattering media using optical coherence tomography," Opt. Express **12**, 4353–4365 (2004).
10. S. Fine and W. P.Hansen, "Optical second harmonic generation in biological systems," Appl. Opt. **10**, 2350–2353 (1971).
11. P. Bianchini and A. Diaspro, "Three-dimensional (3D) backward and forward second harmonic generation (SHG) microscopy of biological tissues," J. Biophotonics **1**, 443–450 (2008).
12. Y. Sun, W. L. Chen, S. J. Lin, S. H. Jee, Y. F. Chen, L. C. Lin, P. T. So, and C. Y. Dong, "Investigating mechanisms of collagen thermal denaturation by high resolution second-harmonic generation imaging," Biophys. J. **91**, 2620–2625

(2006).

13. M. Oliveira dos Santos, V. Bianchini Pelegati, C. Lenz Cesar, T. M. Tenório Zorn, and D. Zezell, "Imaging of third-degree burned skin by two-photon emission fluorescence microscope and second harmonic generation microscopy," *Latin America Optics and Photonics Conference,* OSA Technical Digest (CD) (Optical Society of America, 2010), paper TuE2.

14. N. J. Crane and E. a. Elster, "Vibrational spectroscopy: A tool being developed for the noninvasive monitoring of wound healing." J. Biomed. Opt. **17**, 010902 (2012).

15. M. J. Baker, J. Trevisan, P. Bassan, R. Bhargava, H. J. Butler, K. M. Dorling, P. R. Fielden, S. W. Fogarty, N. J. Fullwood, K. a. Heys, C. Hughes, P. Lasch, P. L. Martin-Hirsch, B. Obinaju, G. D. Sockalingum, J. Sule-Suso, R. J. Strong, M. J. Walsh, B. R. Wood, P. Gardner, and F. L. Martin, "Using fourier transform ir spectroscopy to analyze biological materials." Nat. Protoc. **9**, 1771–91 (2014).

16. D. Elder, R. Elenitsas, C. Jaworsky, and J. Bernett Johson, *Lever's histopathology of the skin, eighth edition*, Human pathology (Elsevier, 1998). Vol. 29.

17. V. Kumar, A. K. Abbas, J. C. Aster, and S. L. Robbins, *Robbins basic pathology*, 9th ed (Elsevier/Saunders, 2013).

18. J. M. Schmitt, A. Knuttel, and R. F. Bonner, "Measurement of optical properties of biological tissues by low-coherence reflectometry," Appl. Opt. **32**, 6032–6042 (1993).

19. S. Ishida and N. Nishizawa, "Quantitative comparison of contrast and imaging depth of ultrahigh-resolution optical coherence tomography images in 800–1700 nm wavelength region," Biomed. Opt. Express **3**, 282–294 (2012).

20. R. Pankov and K. M. Yamada, "Fibronectin at a glance," J. Cell. Sci. **115**, 3861–3863 (2002).

21. A. Barth, "Infrared spectroscopy of proteins," BBA-Bioenergetics **1767**, 1073–1101 (2007).

22. P. Lasch and D. Naumann, "Infrared spectroscopy in microbiology," in *Encyclopedia of analytical chemistry*. (John Wiley & Sons, Ltd, 2006).

23. H. A. Green, Y. Domankevitz, and N. S. Nishioka, "Pulsed carbon dioxide laser ablation of burned skin: In vitro and in vivo analysis," Laser Surg. Med. **10**, 476–484 (1990).

24. A. P. B. S. Campelo, M. W. S. Campelo, G. A. d. C. Britto, A. P. Ayala, S. B. Guimarães, and P. R. L. d. Vasconcelos, "An optimized animal model for partial and total skin thickness burns studies," Acta Cir. Bras. **26**, 38–42 (2011).

25. D. K. Meyerholz, T. L. Piester, J. C. Sokolich, G. K. Zamba, and T. D. Light, "Morphological parameters for assessment of burn severity in an acute burn injury rat model," J. Exp. Pathol. **90**, 26–33 (2009).

26. C. J. Busuioc, F. C. Popescu, G. D.Mogoşanu, I. Lascăr, I. Pirici, O. T.Pop, and L. Mogoantă, "Angiogenesis assessment in experimental third degree skin burns: a histological and immunohistochemical study." Rom. J. Morphol. Embryo. **52**, 887–895 (2011).

27. D. O. Traktuev, S. Merfeld-Clauss, J. Li, M. Kolonin, W. Arap, R. Pasqualini, B. H. Johnstone, and K. L. March, "A population of multipotent cd34-positive adipose stromal cells share pericyte and mesenchymal surface markers, reside in a periendothelial location, and stabilize endothelial networks," Circ. Res. **102**, 77–85 (2008).

28. S. Gronthos, D. M. Franklin, H. A. Leddy, P. G. Robey, R. W. Storms, and J. M. Gimble, "Surface protein characterization of human adipose tissue-derived stromal cells," J. Cell. Physiol. **189**, 54–63 (2001).

29. P. A. Zuk, M. Zhu, P. Ashjian, D. A. De Ugarte, J. I. Huang, H. Mizuno, Z. C. Alfonso, J. K. Fraser, P. Benhaim, and M. H. Hedrick, "Human adipose tissue is a source of multipotent stem cells," Mol. Biol. Cell **13**, 4279–4295 (2002).

30. V. van Harmelen, K. Röhrig, and H. Hauner, "Comparison of proliferation and differentiation capacity of human adipocyte precursor cells from the omental and subcutaneous adipose tissue depot of obese subjects," Metabolism **53**, 632–637 (2004).

31. J. Case, T. L. Horvath, J. C. Howell, M. C. Yoder, K. L. March, and E. F. Srour, "Clonal multilineage differentiation of murine common pluripotent stem cells isolated from skeletal muscle and adipose stromal cells," Ann. NY. Acad. Sci. **1044**, 183–200 (2005).

32. F. Guilak, K. E. Lott, H. A. Awad, Q. Cao, K. C. Hicok, B. Fermor, and J. M. Gimble, "Clonal analysis of the differentiation potential of human adipose-derived adult stem cells," J. Cell. Physiol. **206**, 229–237 (2006).

33. D. T. Furuya, A. C. Poletto, R. R. Favaro, J. O. Martins, T. M. Zorn, and U. F. Machado, "Anti-inflammatory effect of atorvastatin ameliorates insulin resistance in monosodium glutamate–treated obese mice," Metabolism **59**, 395–399 (2010).

34. R. Cancello, C. Henegar, N. Viguerie, S. Taleb, C. Poitou, C. Rouault, M. Coupaye, V. Pelloux, D. Hugol, J. L. Bouillot *et al.*, "Reduction of macrophage infiltration and chemoattractant gene expression changes in white adipose tissue of morbidly obese subjects after surgery-induced weight loss," Diabetes **54**, 2277–2286 (2005).

35. G. S. Hotamisligil, P. Arner, J. F. Caro, R. L. Atkinson, and B. M. Spiegelman, "Increased adipose tissue expression of tumor necrosis factor-alpha in human obesity and insulin resistance." J. Clin. Invest. **95**, 2409 (1995).

36. A. T. Yeh, B. Kao, W. G. Jung, Z. Chen, J. S. Nelson, and B. J. Tromberg, "Imaging wound healing using optical coherence tomography and multiphoton microscopy in an in vitro skin-equivalent tissue model," J. Biomed. Opt. **9**, 248–253 (2004).

37. J. De Boer, S. Srinivas, A. Malekafzali, Z. Chen, and J. Nelson, "Imaging thermally damaged tissue by Polarization Sensitive Optical Coherence Tomography," Opt. Express **3**, 212 (1998).

38. N. Iftimia, R. D. Ferguson, M. Mujat, A. H. Patel, E. Z. Zhang, W. Fox, and M. Rajadhyaksha, "Combined reflectance confocal microscopy/optical coherence tomography imaging for skin burn assessment." Biomed. Opt. Express **4**, 6537–6548 (2014).

39. P. H. Puhakka, J. H. Ylärinne, M. J. Lammi, S. Saarakkala, V. Tiitu, H. Kröger, T. Virén, J. S. Jurvelin, and J. Töyräs,

"Dependence of light attenuation and backscattering on collagen concentration and chondrocyte density in agarose scaffolds," Phys. Med. Biol. **59**, 6537–6548 (2014).

40. Y. Yang, T. Wang, N. C. Biswal, X. Wang, M. Sanders, M. Brewer, and Q. Zhu, "Optical scattering coefficient estimated by optical coherence tomography correlates with collagen content in ovarian tissue," J. Biomed. Opt. **16**, 090504 (2011).

41. R. Tanaka, S.-i. Fukushima, K. Sasaki, Y. Tanaka, H. Murota, T. Matsumoto, K. Matsumoto, T. Araki, and T. Yasui, "In vivo visualization of dermal collagen fiber in skin burn by collagen-sensitive second-harmonic-generation microscopy." J. Biomed. Opt. **18**, 61231 (2013).

42. M.-G. Lin, T.-L. Yang, C.-T. Chiang, H.-C. Kao, J.-N. Lee, W. Lo, S.-H. Jee, Y.-F. Chen, C.-Y. Dong, and S.-J. Lin, "Evaluation of dermal thermal damage by multiphoton autofluorescence and second-harmonic-generation microscopy," J. Biomed. Opt. **11**, 064006–064006–6 (2006).

43. S. Bancelin, A. Nazac, B. H. Ibrahim, P. Dokládal, E. Decenciere, B. Teig, H. Haddad, H. Fernandez, M. C. Schanne-Klein, and A. De Martino, "Determination of collagen fiber orientation in histological slides using Mueller microscopy and validation by second harmonic generation imaging." Opt. Express **22**, 22561–22574 (2014).

44. R. Ambekar, T. Y. Lau, M. Walsh, R. Bhargava, and K. C.Toussaint, Jr., "Quantifying collagen structure in breast biopsies using second-harmonic generation imaging," Biomed. Opt. Express **3**, 2021–2035 (2012).

1. Introduction

In 2016, in the United States alone, 486,000 patients received medical treatment for skin burns and 3,275 died from their injuries [1]. Burn injuries are the third largest cause of accidental deaths in the USA. Despite the advances in the evaluation and treatment of skin burns, infection remains the main cause of morbidity and mortality. An infected lesion not only heals more slowly but can also lead to systemic infection and prevents proper skin graft.

The current skin burn management includes three steps of evaluation, treatment and rehabilitation. The gravity of the injury is assessed according to wound depth, localization and area, and classifies the injuries into first, second or third degree burns. Third degree burn is characterized by achieving the whole depth of the dermis, and may reach the muscle tissue. Skin exposure to heat for a long period causes disruption of collagen fibers affecting their organization in the dermis, destruction of dermal appendages, as well as epithelial necrosis [2]. During the healing process, the extracellular matrix forms a mechanical supporting scaffold made of collagen, elastin and glycoproteins that regulates cell proliferation and differentiation for tissue regeneration [3].

Determination of the wound depth is a key factor to choose the adequate treatment, as the skin regeneration processes of wound contraction and re-epithelization will depend on it. A subjective evaluation is done by the surgeon, who will take into account the burn appearance, color, blood perfusion and feeling to the touch. Histological analysis is the gold standard evaluation; however it is not always performed as it is time-consuming and requires an experienced pathologist. Treatment is performed after complete wound evaluation and cleaning. In recent decades, novel methods of debridement of burned tissue and skin grafting have been introduced in hospitals, leading to a reduction in mortality rates. Debridement of the lesion is a burned tissue removal process that enables proper evaluation of the base of the lesion and promote healing [4]. In recent years, lasers have been used to successfully remove biological tissue; they could thus also be used to treat skin burns.

There are basically two types of tissue removal by laser: thermal ablation and plasma ablation. In both processes, the laser energy is absorbed by the tissue. Thermal ablation induces a temperature rise in the tissue, leading to evaporation and thermal damage to the neighboring tissue. In plasma mediated ablation, the tissue is sublimated, carrying away most of the laser energy [5], thus practically eliminating thermal damage to the remaining tissue. This can be achieved using ultra-short lasers pulses and has the advantage of being fast and causing almost no bleeding.

In this study, we compare the healing processes of burned skin treated by debridement or by ultra-short high intensity femtosecond laser pulses, by focusing on collagen quantity and organization. For this purpose, we combine four different methods for *in vivo* and *ex vivo* collagen characterization: gold standard histopathology, Optical Coherence Tomography,

Second-Harmonic Generation, and Fourier Transform Infrared spectroscopy.

Optical Coherence Tomography (OCT) is a novel non-invasive optical technique that can perform *in vivo* 3D imaging of biological tissues. Introduced in the nineties, it is now routinely used in ophthalmology and cardiology, and is being proven to be useful as well in gastroenterology, dentistry, and dermatology [6]. OCT is the equivalent of echography using light waves instead of ultrasound waves, with a resulting resolution that is 10 to 100 times higher than US, MRI or CT, and approaching the level of histology. OCT is based on low-coherence interferometry: light backscattered from the tissue is combined with light reflected in a reference arm in order to create an interference pattern. The resulting interferogram forms an optical cross-section revealing the morphological structures of the tissue. Then, two-dimensional and three-dimensional images can be reconstructed with transversal x and y scanning. An OCT system using a low-power source such as a laser or a LED in the visible and near-infrared range can typically image at a depth of 1mm in the skin [7]. Furthermore, the OCT signal can be used to extract the optical attenuation coefficient of the tissue, which quantifies the scattering and absorption phenomena and can give valuable information about the state of the tissue [8, 9].

Second-Harmonic Generation (SHG) microscopy is a non-linear microscopy technique, i.e., based on non-linear light-matter interactions. It can image biological samples without exogenous labeling. Depending upon the experimental circumstances this technique can be invasive (when tissue samples have to be cut prior to imaging), or non-invasive (when imaging is taken *in vivo*). It is a powerful tool to investigate the components of cells and extracellular matrix, in particular the fibrillar network consisting of collagen and elastin. SHG is a non-linear process in which two photons passing through some particular structures generate only one photon with twice the energy. This non-linear event has a very low probability so that the density of energy on the tissue has to be high enough in compensation. It requires a high density of energy on the tissue, which is achieved with ultra-short laser pulses of high intensity and low average power; but is still compatible with biological imaging at shallow depths. The structures capable of emitting SHG light are non-centrosymmetric structures such as collagen in biological tissues [10–13], so that SHG microscopy is well-suited to monitor the evolution of collagen components inside the tissue and thus its healing process.

Fourier Transform Infrared spectroscopy is an optical technique that provides biochemical information on a thin slice sample exposed to infrared radiation. The molecules of the sample selectively absorb radiation of those specific wavelengths that cause non-zero changes of dipolar moment. Consequently, the vibrational energy levels transfer from ground state to excited state, an energy transition that is specific of a given chemical compound in a given environment. In this work the FTIR was used to monitor the collagen during the healing process [14, 15].

2. Material and methods

2.1. Animal model

A third degree or full-thickness burn reaches both epidermis and dermis. Macroscopically it appears as white, with texture similar to leather, or carbonized, dry and anesthetic due to the destruction of nerve endings [16, 17]. Histologically, the devitalized tissue has thrombosis capillary endothelium damage, leading to ischemia-induced cell death. In our study, the third degree burns were obtained by vapour exposure.

The study was conducted on 20 male Wistar rats of approximately 300 g. All rats were housed and fed properly in individual cages under controlled conditions of temperature and light regime of 12h/12h. Throughout the experiment, they received water and solid ration ad libitum.

On day 0, the animals were intramuscularly anesthetized with a combination of ketamine hydrochloride (0.32 mL/kg) and xylazine (0.2 mL/kg), then trichotomy and antisepsis was performed in the dorsal region. Third-degree skin burns on 3 areas were induced by exposure to a source of water vapor at 90 °C with a 8 mm-diameter for 10 seconds. The histological analysis

confirmed that there was a third degree burn on total thickness involving total necrosis of the epidermis and dermis of rats. Macroscopic views of the skin burns are shown on Fig. 1.
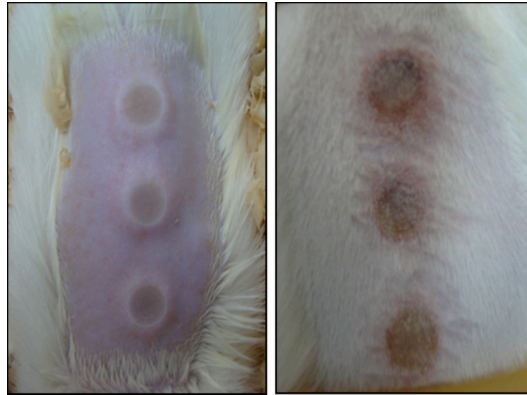

Fig. 1. Aspect of burned skin on rat dorsal area.

The wound treatments were performed three days after the burn: the first area was irradiated with a laser, the second area with surgical debridement, the third area was the control area. Before each procedure, an aqueous solution of chlorhexidine 2% was applied on the lesion for disinfection. The animals were randomly distributed into 4 groups of 5 animals, with 5 different sacrifice intervals, at 3, 5, 7 and 14 days post-treatment.

The animal protocol is in accordance with the standards for scientific vivisection of animals (Law no. 6638, of May 08 of 1979) and the ethical principles of animal experimentation. This project was approved by the Ethics Committee for Animal Research of the Institute of Energy and Nuclear Research (Nº 29/CEPA-IPEN/SP).

2.2.　Burn treatments

Surgical debridement was performed by scraping the burned skin with a cold blade until the beginning of bleeding. For plasma-mediated laser ablation, this study used ultrashort pulses from an Ti:Sapphire laser system composed by a Femtopower Compact PRO amplifier seeded by a Rainbow main oscillator, both from Femtolasers. This system generated 90 fs, 785 nm centered pulses, in a 2 kHz repetition rate train, with a maximum pulse energy of 800 μJ (table 1). A pilot study was carried out to evaluate the tissue removal promoted by these ultrashort pulses, attenuating their energy to 5, 10, 20 and 50 μJ, and focusing the laser beam by a f=50 mm lens on the burned region of *ex vivo* skin of male Wistar rat samples, resulting in a laser spot size of 24 μm. The samples were fixed on an acrylic sheet and positioned on a table with computer controlled micrometric two-axis displacement in the plane orthogonal to the laser beam. The irradiation was performed by scanning a region of 1x2 mm^2 with 540 mm/min sample displacement speed, which produced a 25% spatial pulse overlapping. The effects of the 4 different energy conditions were evaluated using OCT imaging. The pilot study showed that the 10 μJ pulses produced the best results, so this energy was chosen to promote the ablation of burned tissue *in vivo*. Respiratory motion can be problematic for *in vivo* tissue removal in animals, as it produces relative displacements between the beam focus and the animal skin surface. Thus, we chose to position the beam focus between 150 and 200 μm below the skin surface when the rat inspired air. We concluded that 10 μJ pulses ensure a sufficient tissue removal depth even in the presence of breathing artifacts.

Table 1. Laser Parameters

Parameters	Quantities
Frequency	2 kHz
Pulse Duration	90 fs
Wavelength	785 nm
Rayleigh range	0.576 mm
Spot size	24 μm
Energy per pulse	10 μJ

2.3. Histopathology analysis

The animals were randomly sacrificed with lethal doses of anesthetics on days 3, 5, 7 and 14 post-treatment. For each region (burned skin, ablated skin, debrided skin), skin samples from each one of the 3 areas were carefully removed with a scalpel, in order to involve the whole wound area and depth as well as some healthy skin adjacent to the wound edged. Part of the samples were then cut in 5 μm thick slices, fixed in Methacarn (methanol solution with Carnoy) for a maximum period of 3h, and stained with classical Hematoxylin and Eosin (H&E). The rest of the bulk tissue was prepared and used for non-linear microscopy. They were mounted on glass slides and covered with coverslip for examination under light microscope (Leica DMLP, Germany). The histopathology analysis was then performed by a pathologist.

2.4. OCT imaging

The OCT system used for this study is the Fourier-Domain OCP930SR model from Thorlabs Inc., USA. Its source is a 930 nm centered LED with a 100 nm bandwidth. It provides axial and lateral resolution in air of 6.0 μm, which means around 8 μm in the tissue, with a frame rate of 8fps. The generated images contain 2048 x 512 pixels, corresponding to 6 x 1.5 mm^2.

   OCT imaging was performed *in vivo* just before sacrifice of the animal, at 3, 5, 7 and 14 days after treatment. Direct visual examination of the OCT images was performed, as well as optical attenuation calculation. Figure 2 shows a typical image of healthy skin and one corresponding depth profile of the signal.
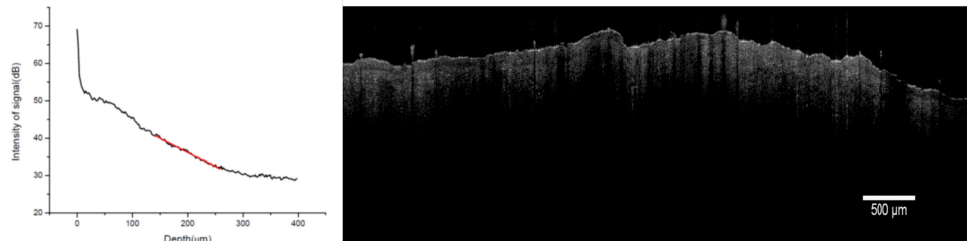

Fig. 2. Typical OCT image of normal skin and intensity curve of the OCT signal with depth on a region of interest of width 1500 μm.

   The region of dermis was delineated on the morphological OCT image and the attenuation profile of the optical signal with depth was extracted for each region using LabVIEW software.The model for the amplitude of the signal in decibels is described in Eq. (1) [18, 19].

$$10\log\left(\frac{P(z)}{P_0}\right) \approx -20\mu_a \log(ez) + 10\exp(K\mu_s A(z)) \tag{1}$$

where P_0 is the incident power on the surface of the sample, P(z) is the backscattered power from a depth z in the tissue, K is a constant that depends on the coherence function of the

source, A(z) is the beam divergence function, μ_s and μ_a are the scattering and total attenuation coefficients, respectively.

For each sample, the arithmetic mean of the attenuation coefficients μ_a of each depth profile was calculated. Then, for each rat we considered the ratios between healthy skin, burned skin, laser-irradiated skin and debrided skin.

2.5. SHG imaging

The samples were cryosectioned perpendicular to the epidermal layer comprising a transverse cross section of the epidermal and dermal layers, of 20 μm thickness, and bathed in isopentane for cryopreservation and stored in liquid nitrogen (-196 °C). The tissue slices without exogenous marker were then examined with a confocal microscope LSM 780 NLO-Zeiss Axio Observer (Carl Zeiss AG, Germany), using 10x and 40x objectives, from the the National Institute of Science and Technology Photonics Applied to Cell Biology (INFABIC), at the State University of Campinas, Brazil. Images were collected using a Mai Tai ultra-short pulsed laser from Spectra Physics, with a center wavelength of 950 nm for excitation and a low pass filter of 485 nm for detection of SHG signal. The images have 512x512 pixels.

The SHG images were further analyzed by Fast Fourier Transform (FFT), ImageJ 1.45 software (National Institutes of Health, USA) to calculate the Collagen Orientation Index (COI). The COI is defined in Eq. (2).

$$COI = 1 - \frac{W}{H} \tag{2}$$

where W and H represent the width and height of the ellipse or circle in the power plots of SHG images. The COI ranges from 0 to 1; it approaches 1 for collagen fibers with parallel orientations, 0 for collagen fibers with random orientations.

For each sample, three regions of interest, measuring 25 μm of size, were delimited around 200 μm below the outermost layer of the epithelium, to perform FFT. The fields of view were not continuous in all samples of the groups, thus the arithmetic mean of the COI was calculated to identify the similarities and differences between the groups of burned, debrided and irradiated skin.

2.6. FTIR spectroscopy

The spectra were obtained with a commercial FTIR system (model 6700, Nicolet Instruments, USA), equipped with a μATR (Micro Attenuated Internal Reflectance) sample device. During the μATR-FTIR measurements, samples were pressed onto a diamond crystal (refraction index of 2.41) and irradiated at a 45° incidence angle. For the acquisition of one spectrum, 64 scans were averaged with a sampling interval of 6 cm^{-1}, wavenumbers ranging from 4000 to 800 cm^{-1}.

Analysis of the spectra was performed using MatLab®R2015a (MathWorks®, EUA) software. The fingerprint region between 900 to 1800 cm^{-1} was separated, spectra corrected with the baseline procedure and normalized by amide I intensity band [15]. For signal-smoothing, spectra were submitted to Savitzky-Golay filter with a polynomial of second order in an fifteen points window.

3. Results

3.1. Characterization of the samples by histology

In H&E stained cells, the nucleus present a blue-purple colour due to the nucleic acids colored by Hematoxylin. Proteins from the cytoplasm of the cell, mainly collagen fibers, are colored by Eosin in shades ranging from pink to red (Fig. 3). The junction between the epidermis and the dermis is regular, with no protrusions or indentations. The dermal papillae, which characterizes

the epithelium of rats, the hair follicles and their germinal part are present in tangential slices. The papillary dermis is thin and consists of loose connective tissue. The deeper reticular dermis presents thicker and more abundant collagen fibers, as well as blood vessels.
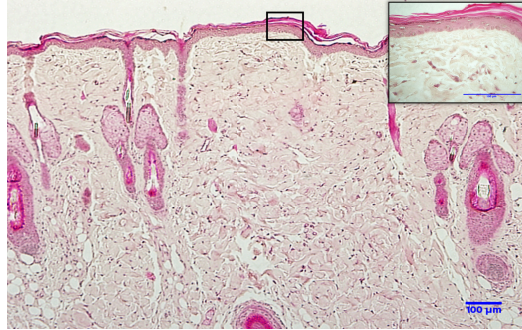

Fig. 3. Histological section of normal skin of the back of a Wistar rat stained with H&E. Structure of normal skin with layers of epidermis and dermis; magnification 20x. In the detail, epidermis and keratinocytes are observed in stages of differentiation; dermis shows the usual distribution of collagen fiber bundles. Magnification 60x.

Histological sections of burned, debrided and ablated skin at days 3 and 14 after vapour exposure are shown in Fig. 4. The third degree burn reached the full thickness of the dermis, degrading the collagen fibers of the reticular dermis layer, destroying the structures and skeletal muscles of the tissue.
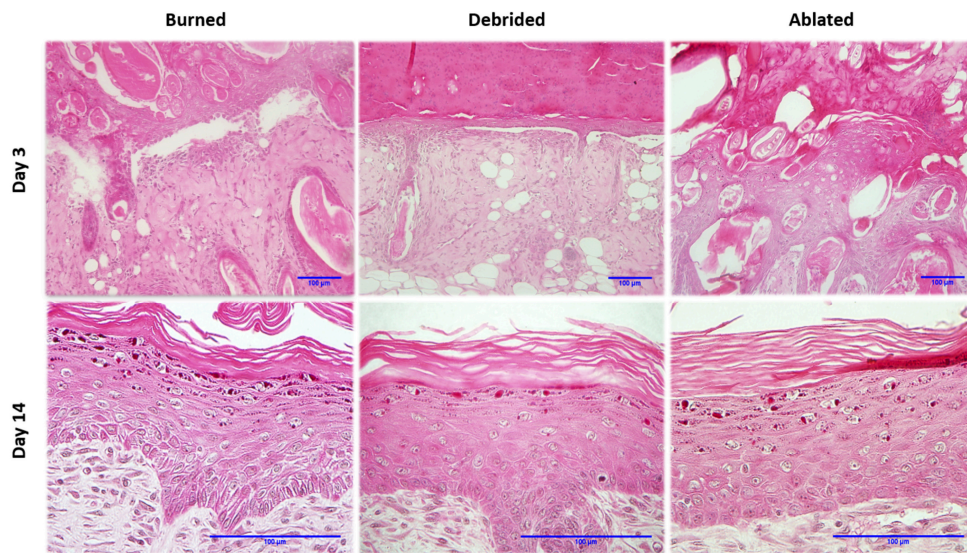

Fig. 4. Left to right: H&E histological sections of burned, debrided and ablated skin at days 3 and 14 after vapour source exposure. At day 3, there is no boundary between the epidermis and dermis layers; a considerable amount of hair follicles having different cross-sections are present. Magnification 20x. At day 14, there is no differences between the samples. Magnification 60x.

On day 3, the lesion is covered with a crust, followed by a complete disruption of the epithelium. Striated skeletal muscle is absent, hair follicles are scattered throughout the dermis, and some

are even found in the epithelium. The epithelium does not have a defined cellular organization and contains some adipocytes. On day 5, the crust is thinner and the skin presents an initial regeneration of keratinized stratified epithelium. The dermis has many fibroblasts with elongated nuclei. Necrotic tissue without vascularization is found in the central area of the lesions, recruiting macrophages and participating in the inflammatory process. On day 7, a keratin layer is forming. A high number of fibroblasts with elongated nuclei is observed in the dermis; skeletal muscle tissue is regenerating. Some hair follicles are found scattered throughout the dermis. On day 14, the epithelium is regenerated and hyper-keratinized. The uniform dermis presents a cellularized dense connective tissue without dermal appendages; and quiescent fibroblasts with elongated nucleus in the final stage of healing process.

All 3 experimental groups reached the same healing stage at day 14 after burn induction.

3.2. OCT analysis of optical attenuation

The OCT images of skin burn tissue were compared to that of healthy skin. The morphological image confirms that the signal reached a deep region of the dermis, at 1 mm of depth. There is a high reflective signal on the surface of the skin at the interface with air, with an intensity peak of 20 dB. The signal intensity then decreases inside the tissue as the photons are scattered by the deeper layers of the skin. The total attenuation coefficient measured in healthy skin was (0.099 ± 0.030) μm^{-1}. Figure 5 shows *in vivo* OCT images of each experimental groups at days 3 and 14 after vapour exposure.

On day 3, the surface presents an uneven crust and increased backreflection due to necrotic tissue. Because of this high backreflection signal, it is impossible to observe the deeper skin layers. However, the surface signal decreases in the following days due to partial regeneration of the epithelium. On day 5, the surface remains uneven, without observation of other skin layers or dermal appendages. On day 7, the dermis appears more uniform, but the epithelium layer remains absent. On day 14, the tissue presents no crust, a more regular surface and a regenerated epithelium (arrows on Fig. 5) .
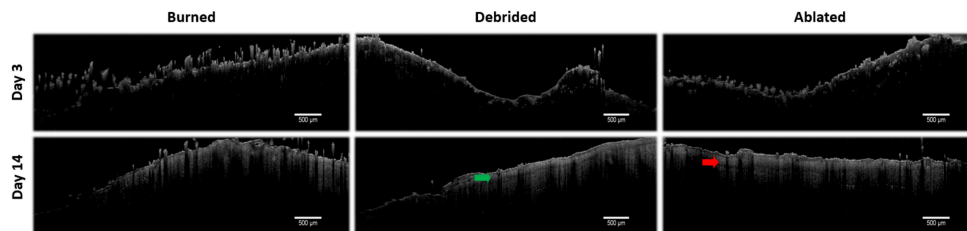

Fig. 5. OCT images of *in vivo* rat skin tissues from the 3 experimental groups at days 3 and 14 after vapour exposure. Arrows show the regenerated epithelium.

Beyond morphological evaluation, the optical attenuation coefficient was also evaluated by OCT. This coefficient quantifies the scattering and absorption phenomena inside the tissue. The value obtained for normal skin was taken as a reference value for comparison, set as 1. Indeed, although quantitative measurement of the coefficient is theoretically possible, it was found that it was experimentally difficult. The measurement was made *in vivo* so that the tissue undergoes contractions and stretches because of the respiratory cycle of the animal. It is thus impossible to normalize the acquisition conditions for all samples.

The attenuation coefficient of ablated skin presents a high increase on day 3. This can be due to an increase in absorption by hemoglobin at 930 nm. Indeed, surgical debridement exposes the tissue to promote healing; during this process, blood vessels are exposed near the surface. This effect is less observed with laser ablation thanks to a more precise control of the depth of

treatment by gradual irradiation.

None of the three groups reached the initial value of 1 at day 14 after vapour exposure. However, the attenuation curve of laser-ablated skin converges towards a value closer to that of normal skin than those of untreated or debrided skin, as shown by statistical analysis with Dunn test at 5% significance using GraphPad Prism 5 software. No statistical difference in attenuation coefficient is measured between the normal skin and laser ablated skin at day 14, while debrided skin and burned skin remain statistically different from normal skin.

3.3. SHG characterization for collagen orientation

Figure 6 shows typical SHG images in the dermis, where collagen appears in red. The dark regions in the image are structures that do not generate SHG signal.
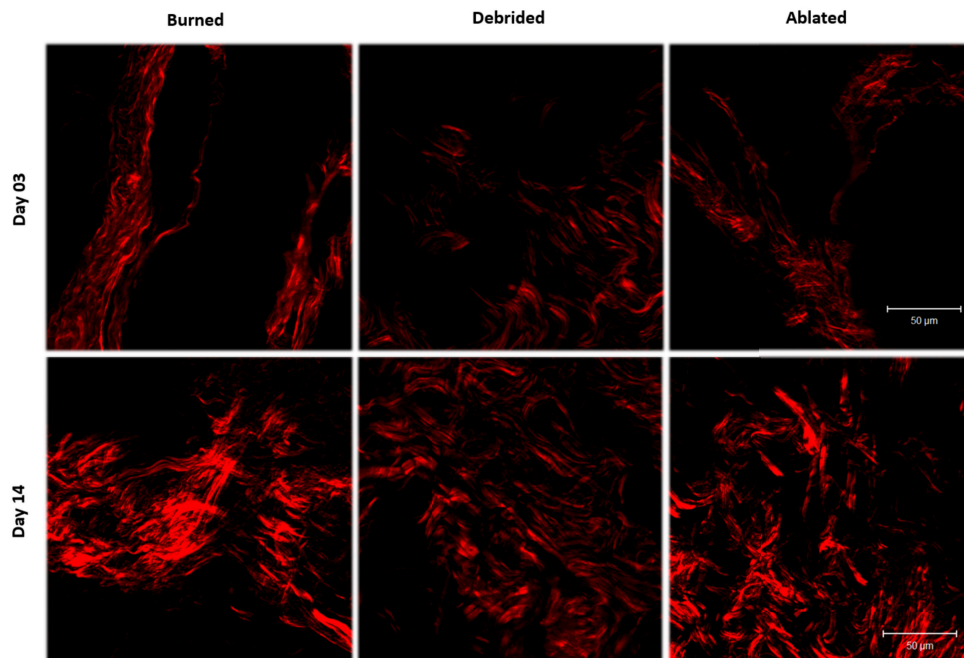

Fig. 6. SHG images, perpendicular sections of 20 μm thickness of skin burn tissue dermis samples at days 3 and 14, showing the localization of the collagen fibers in red.

SHG reveals the distribution of collagen in the extracellular matrix (ECM), an indicator of the skin regeneration process. We observe a qualitative increase of collagen distribution over time. This is due to fibroblasts that restore the mechanical stability of the connective tissue injury, producing collagen, elastin and proteoglicans [20]. However, the morphological collagen structure is changed, along with the healing process.
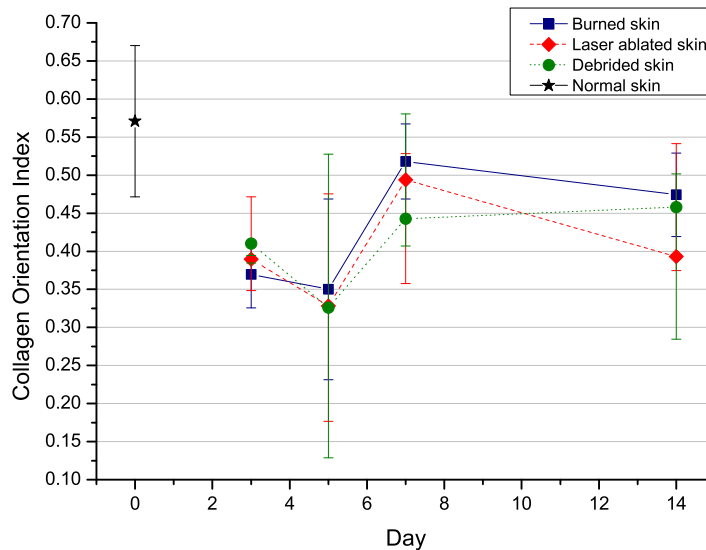
Fig. 7. Evolution of the COI, Collagen Organization Index, for each experimental group at days 3, 5, 7 and 14 after vapour exposure.

Figure 7 shows the evolution of the Collagen Organization Index over time (0 represents totally desorganized fibers, while 1 represents parallel fibers). It can be observed that the orientation of collagen has an equal behavior curve for all samples during the follow-up period of the regeneration process.

On day 3, the collagen orientation is random. This phase of the healing process does not involve dermal collagen regeneration. The characteristics of this phase are homeostasis, coagulation, activation of local immune response, phagocytosis and cell migration. The inflammatory phase can last more than three days, depending on the severity of the injury, as is the case in this study, where the lesion reached the muscle region. On day 5, the collagen orientation remains largely unchanged. On day 7, the collagen is much more organized during the proliferative phase characterized by vascular reconstruction and generation of granular tissue. At this stage, the underlying dermis shrinks and brings the edges of the wound closer one to another. Fibroblasts are stimulated by the growth factor levels of local derivative (PDGF) and transforming growth factors, begin to proliferate and infiltrate the blood clot, depositing type III collagen and other components of extracellular matrix. On day 14, there is a decrease in the collagen orientation curve. After the peak of collagen proliferation, the maturation of the fibers and differentiation of fibroblasts into myofibroblasts cause contraction of the lesion and its closure. The final values indicate that, even though the lesion has closed, the subdermal regeneration is still not complete.

3.4. FTIR measurements

The functional diagnostics of the burned skin depends on the burn depths and healing stage. In this sense, the skin recovery performance of the three groups was characterized by μATR-FTIR spectroscopy. The healing process vary considerably among the days and its behavior were evaluated through spectral groups intensities. The Fig. 8 shows the debrided spectra compared with healthy skin during the healing process.
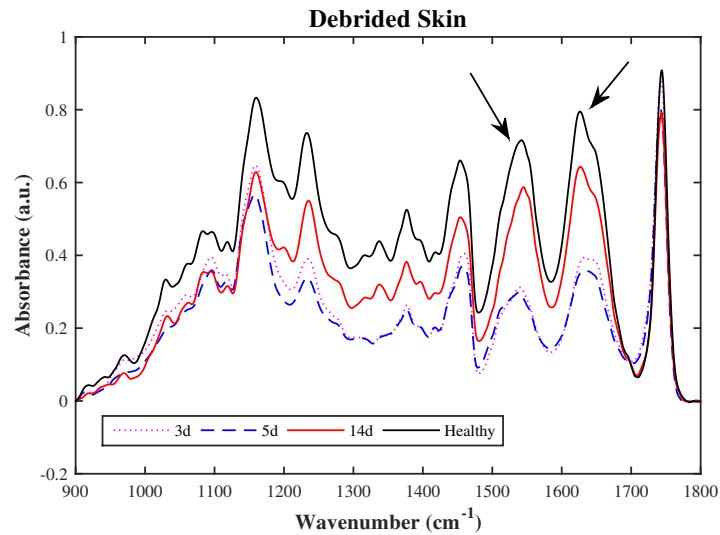
Fig. 8. FTIR mean spectra of debrided skin compared with the healthy skin.

Throughout the healing process, the laser ablated group has demonstrated faster recovery skin performance than the debrided group. Their spectra comparison can provide information for the best choice of treatment, as shown in Fig. 9.
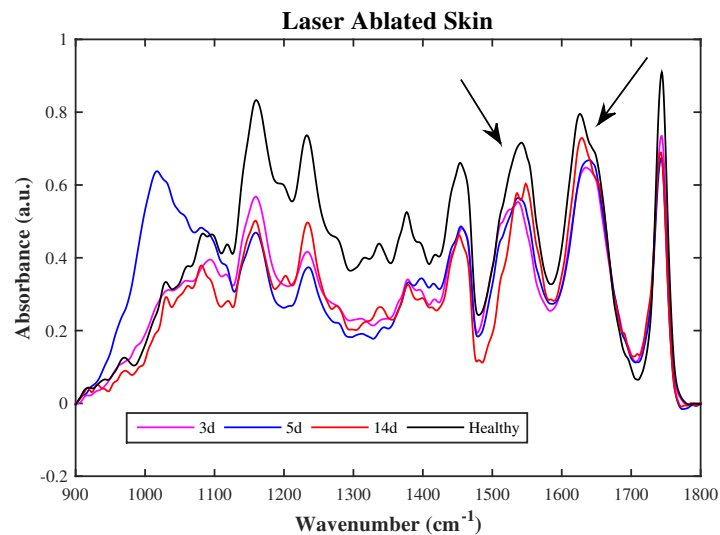

Fig. 9. FTIR mean spectra of ablated skin compared with the healthy skin.

As shown in the Fig. 8 and 9, the debrided spectra show significantly more slow recovery in the 1500 cm^{-1} to 1700 cm^{-1} than the laser ablated spectra. This region is related to the main collagen bands. The absorption peaks of amides indicate peptide bonding in protein, then the vibrational mode associated to parallel β-sheet [21] increased quicker in ablated skin than debrided skin suggesting that laser ablation may have earlier healing process. The 900 cm^{-1} to 1200 cm^{-1}

region of biological samples FTIR spectra is generally dominated by the symmetrical stretching of PO_2^- in the nucleic acid and C-O-C and C-O-P stretching of oligo and polysaccharides [22]. There is presence of adipocytes scattered throughout the dermis, related to the vascularization and fastening of perfusion, between the 3rd and 7th day, mainly on the laser ablated tissue on the 5th day. This fact makes possible to the epidermal cells interact with a variety of extracellular-matrix proteins that are interspersed with stromal type I collagen at the margin of the wound. This observation is remarkable and can be very useful for burned skin treatment.

4. Discussion

The use of lasers for removing skin burn debris and necrotic tissue has few studies in the literature [23]. Our results concerning burned skin wound depth and healing phases are comparable to prior works [24–26].

Three monitoring modalities used in the study, histology, OCT, and SHG, found that the healing processes with surgical debridement or laser ablation treatments are equivalent, and the FTIR results suggests that laser ablation may have earlier healing process than scalpel debridement of burned skin.

A remarkable characteristic of the tissue angiogenesis process revealed by histology is the presence of adipocytes scattered throughout the dermis. These cells are CD34-positive progenitor cells, that have a role in restoring damaged vascular networks following trauma, burns or tumors [26]. A study by Traktuev [27] demonstrated that stromal cells derived from subcutaneous adipose tissue, which have properties of preadipocytes and manifest clonal pluripotency along multiple lineage pathways [28–32], have structural and functional characteristics of pericytes within the adipose tissue. This finding shed a unique light on their importance in normal adipose biology as well as a biological basis for their ability to promote vascularization and accelerate tissue perfusion. Studies with fat mice have shown increased adipose tissue infiltration of macrophages and pro-inflammatory cytokines [33]. Human studies have also reported similar results of recruitment of macrophages by adipocytes [34, 35].

In previous literature on skin burns assessment, OCT had mainly been used with a polarization sensitive setup for collagen imaging [36–38], but no measurement of the optical attenuation coefficient had been reported. However, other OCT studies found that low attenuation is correlated with low collagen content, in the case of agarose scaffolds [39] and *ex vivo* ovarian tissue [40], which is consistent with our results.

Several studies using non-linear optical microscopy technique for collagen imaging have been reported on skin burns [41, 42], but not on collagen orientation quantification. Collagen fibers orientation have been studied on *ex vivo* uterine cervial tissue with SHG [43] and breast tumor tissue with polarization-resolved SHG [44]. Tanaka et al. found that skin burn tissue presents molten and fibrous structures of dermal collagen [41], which is consistent with our finding on Fig. 7. After thermal damage, the burned skin tissue presents collagen fibers less organized than in normal tissue, which can be due to the presence of molten collagen fibers. After a week, the dermis is regenerating with more organized fibrous collagen.

In this work, we tackled the problem of assist medical doctor to choose the best treatment for burned skin. Our experiment with μATR-FTIR showed that the debrided and ablated skin spectra provide different healing process. The recognition of dissimilar peaks presence does not fully describe the biological complexity of burn wound healing. Our findings indicated an increase in amide II band and corroborates to interpretation for most pronounced protein expression, which may be explained by the quickest recovery when necrotic tissue was removed by laser ablation.

5. Conclusion

In this study, the skin healing process was characterized by histology examination, OCT measurement of optical attenuation coefficient, SHG measurement of collagen orientation, FTIR

spectroscopy to assess the amide II content. The histology, OCT and SHG results indicates that high-intensity femtosecond lasers showed the same ability for skin burn treatment as surgical debridement, and FTIR results suggests recovery is quickest when necrotic tissue was removed by laser ablation. Pulsed lasers can perform efficient and accurate tissue ablation with reduced thermal residual damage. An energy of 10 μJ / pulse (about 90 femtoseconds temporal width and 2 kHz repetition rate) was sufficient for controlled removal of burned tissue debris and to promote healing on rat skin.

Funding